



HAL
open science

Spectropolarimetric observations of the transiting planetary system of the K dwarf HD 189733

Claire Moutou, Jean-François Donati, Renaud Savalle, Gaïte Hussain, Evelyne Alecian, François Bouchy, Claude Catala, A. C. Cameron, Stéphane Udry, A. Vidal-Madjar

► **To cite this version:**

Claire Moutou, Jean-François Donati, Renaud Savalle, Gaïte Hussain, Evelyne Alecian, et al.. Spectropolarimetric observations of the transiting planetary system of the K dwarf HD 189733. *Astronomy and Astrophysics - A&A*, 2007, 473, pp.651-660. 10.1051/0004-6361:20077795 . hal-03732592

HAL Id: hal-03732592

<https://hal.science/hal-03732592>

Submitted on 6 Sep 2022

HAL is a multi-disciplinary open access archive for the deposit and dissemination of scientific research documents, whether they are published or not. The documents may come from teaching and research institutions in France or abroad, or from public or private research centers.

L'archive ouverte pluridisciplinaire **HAL**, est destinée au dépôt et à la diffusion de documents scientifiques de niveau recherche, publiés ou non, émanant des établissements d'enseignement et de recherche français ou étrangers, des laboratoires publics ou privés.

Spectropolarimetric observations of the transiting planetary system of the K dwarf HD 189733[★]

C. Moutou¹, J.-F. Donati², R. Savalle¹, G. Hussain³, E. Alecian^{4,5}, F. Bouchy⁶, C. Catala⁴, A. Collier Cameron³, S. Udry⁷, and A. Vidal-Madjar⁶

¹ Laboratoire d'Astrophysique de Marseille, CNRS UMR 6110 Traverse du Siphon, 376 Marseille, France
e-mail: Claire.Moutou@oamp.fr

² Laboratoire d'Astrophysique Toulouse-Tarbes, Observatoire Midi Pyrénées, 14 Av. E. Belin, 31400 Toulouse, France

³ School of Physics and Astronomy, University of St Andrews, North Haugh, St Andrews, Fife KY16 9SS, UK

⁴ LESIA, Observatoire de Paris Meudon, Place J. Janssen, 92195 Meudon Cedex, France

⁵ Dept. of Physics, Royal Military College of Canada, PO Box 17000, Stn Forces, Kingston, K7K 7B4, Canada

⁶ Institut d'Astrophysique de Paris, UMR7095 CNRS, Université Pierre & Marie Curie, 98bis Bd Arago, 75014 Paris, France

⁷ Observatoire de Genève, 51 ch. des Maillettes, 1290 Sauverny, Switzerland

Received 4 May 2007 / Accepted 12 July 2007

ABSTRACT

Context. With a Jupiter-mass planet orbiting at a distance of only 0.031 AU, the active K2 dwarf HD 189733 is a potential candidate in which to study the magnetospheric interactions of a cool star with its recently-discovered close-orbiting giant planet.

Aims. We decided to explore the strength and topology of the large-scale magnetosphere of HD 189733, as a future benchmark for quantitative studies for models of the star/planet magnetic interactions.

Methods. To this end, we used ESPaDOnS, the new generation spectropolarimeter at the Canada-France-Hawaii 3.6 m telescope, to look for Zeeman circular polarisation signatures in the line profiles of HD 189733 in 2006 June and August.

Results. Zeeman signatures in the line profiles of HD 189733 are clearly detected in all spectra, demonstrating that a field is indeed present at the surface of the star. The Zeeman signatures are not modulated with the planet's orbital period but apparently vary with the stellar rotation cycle. The reconstructed large-scale magnetic field, whose strength reaches a few tens of G, is significantly more complex than that of the Sun; it involves in particular a significant toroidal component and contributions from magnetic multipoles of order up to 5. The Ca II H & K lines clearly feature core emission, whose intensity is apparently varying mostly with rotation phase. Our data suggest that the photosphere and magnetic field of HD 189733 are sheared by a significant amount of differential rotation.

Conclusions. Our initial study confirms that HD 189733 is an optimal target for investigating activity enhancements induced by closely orbiting planets. More data are needed, densely covering both the orbital and rotation cycles, to investigate whether and how much the planet contributes to the overall activity level of HD 189733.

Key words. stars: individual: HD189733 – planetary systems – techniques: polarimetric – techniques: spectroscopic – stars: magnetic fields – stars: activity

1. Introduction

Planetary systems characterized by a giant planet at a few stellar radii from their parent stars (known as hot Jupiters) currently make up ~20% of all known extrasolar planets. Spectroscopic observations of stars hosting hot Jupiters recently revealed that chromospheric activity indices (such as core emission in Ca II H&K and infrared triplet lines) are sometimes modulated with the orbital period of the giant planet (rather than with the rotation period of the star), suggesting that such giant planets may significantly boost the activity level of the host star (Cuntz et al. 2000; Shkolnik et al. 2003, 2005). According to theoreticians (e.g., Cuntz et al. 2000; Ip et al. 2004), this modulation could result either from tidal effects (enhancing local dynamo action and activity at the surface of the star) or from magnetospheric

interaction between the host star and its close-in planet (inducing reconnection events as the planet travels through the large magnetic loops anchored in the stellar surface). If due to reconnection, the resulting activity should depend mostly on the large-scale magnetic field of the host star, on the planet's magnetic field and on the orbital distance with respect to the Alfvén radius of the host star; if due to tidal effects, the excess activity may indicate the presence of a “surface wave” of small-scale magnetic features comoving with the planet orbital motion and resulting from local turbulence and dynamo action enhancements induced by the planet pass-by. Photometric observations by the MOST space telescope of several hot-Jupiter systems suggest that stellar surface activity, in the form of cool spots comoving with the planet orbital motion, could indeed be caused by the close-in giant planet (Walker et al. 2006); if confirmed, it would provide additional evidence for magnetic interactions between giant planets and their host stars. Magnetic fields were also recently invoked as a possible formation mechanism for giant planets in close orbits around Sun-like stars (Kurucz 2007).

[★] Based on observations obtained at the Canada-France-Hawaii Telescope (CFHT) which is operated by the National Research Council of Canada, the Institut National des Sciences de l'Univers of the Centre National de la Recherche Scientifique of France, and the University of Hawaii.

Very recent observations of τ Boo with the ESPaDOnS spectropolarimeter (Donati et al. 1997; Donati 2007), mounted at the Cassegrain focus of the 3.6 m Canada-France-Hawaii Telescope (CFHT), revealed that surface magnetic fields are indeed present at the surface of planet-hosting stars and can be reliably detected through the Zeeman signatures they generate in spectral line profiles (Catala et al. 2007). Despite a sparse temporal sampling of the rotational cycle, their data demonstrated the feasibility of measuring and mapping large-scale magnetic fields at the surfaces of such stars, opening radically new and extremely promising perspectives for observational studies of the magnetic interactions between active stars and their close-in giant planets. We therefore decided to initiate a new program aimed at detecting and modeling the magnetic topologies of stars hosting close-in giant planets, in order to provide theoretical models of planet-star magnetic interaction with quantitative constraints. With its short orbital period, the transiting planetary system HD 189733, discovered at Observatoire de Haute Provence through both photometric and spectroscopic signatures (Bouchy et al. 2005), is an ideal candidate for our program.

Most parameters of HD 189733 are now tightly constrained, thanks to successive very detailed spectroscopic and photometric monitoring programs (Bouchy et al. 2005; Bakos et al. 2006; Winn et al. 2007b,a). The planet's mass and radius are equal to $1.13 \pm 0.03 M_{\text{Jup}}$ and $1.156 \pm 0.046 R_{\text{Jup}}$ respectively, while its orbital period is 2.2185733 ± 0.0000019 d. The system geometry is also well known, the inclination i of the orbital axis with respect to the line of sight being $85.76 \pm 0.29^\circ$. With a mass, effective temperature and radius respectively equal to $0.82 \pm 0.03 M_{\odot}$, 5050 ± 50 K and $0.753 \pm 0.023 R_{\odot}$, the K2V parent star is slightly metal poor and active, with a line-of-sight projected equatorial rotation velocity $v \sin i = 3.0 \pm 0.2 \text{ km s}^{-1}$. In addition to the photometric eclipses induced by the transiting exoplanet, HD 189733 exhibits intrinsic photometric variability; this is likely the result of its activity and the dark spots on its surface, modulating the amount of light received from the star as rotation carries spots in and out of the observer's view (Hébrard & Lecavelier des Etangs 2006; Winn et al. 2007a; Matthews 2007; Croll et al. 2007). From Hipparcos observations collected over 3 yr, Hébrard & Lecavelier des Etangs (2006) confirm that intrinsic variability is indeed the main source of out-of-eclipse photometric fluctuations on HD 189733, and that these fluctuations are modulated with an average rotation period of 11.8 d. From 93 nights of ground-based photometry secured from 2005 October to 2006 July, Winn et al. (2007a) show that the light curve of HD 189733 is evolving significantly on a timescale of 20 d. Using their last 30 d of observations (showing the highest amplitude modulation), they derive a rotation period of 13.4 ± 0.4 d, significantly longer than that of Hébrard & Lecavelier des Etangs (2006). Nearly-continuous space-based photometry of HD 189733 was obtained over 21 d in July and August 2006 with MOST, only 50 d after the latest observations of Winn et al. (2007a); from these data, the rotation period was found to be 11.8 d to within better than 0.1 d (Matthews 2007; Croll et al. 2007). We suspect that the discrepancy between these different estimates is not due to measurement errors, but rather to temporal variations in the spot pattern coupled to a significant amount of differential rotation over stellar latitudes (e.g., Hall 1991; Catala et al. 2007). We return to this issue later in the paper; in the meantime, we adopt an average rotation period of 11.8 d for HD 189733. Table 1 summarises all relevant system properties that are used in this paper and corresponding references.

Table 1. Star and planet parameters (and associated error bars) for the transiting system HD 189733.

Planet mass (M_{Jup}) ^c	1.13 (0.03)
Planet radius (R_{Jup}) ^b	1.154 (0.032)
Orbital period (d) ^c	2.2185733 (0.0000019)
Semi-major axis (AU) ^c	0.031 (0.001)
Stellar mass (M_{\odot}) ^a	0.82 (0.03)
Stellar radius (R_{\odot}) ^c	0.753 (0.02)
Stellar effective temperature (K) ^a	5050 (50)
Stellar $v \sin i$ (km s^{-1}) ^c	2.97 (0.22)
Stellar rotation period (d) ^d	11.73 (0.07)
Orbit inclination ($^\circ$) ^b	85.76 (0.29)

Corresponding references are: ^a Bouchy et al. (2005), ^b Bakos et al. (2006), ^c Winn et al. (2007b), ^d Croll et al. (2007).

This paper presents the first spectropolarimetric study of HD 189733. Our aim is to detect and monitor the Zeeman signatures in the spectrum of the host star to map its large-scale magnetic topology and study the magnetic interaction between the star and its close-by giant planet. In Sect. 2 we describe the observations, while in Sect. 3 we detail the modeling of the spectropolarimetric data. We discuss the activity level of the star and its possible variation with orbital and rotational phase in Sect. 4. In Sect. 5 we examine spectra taken during transit for potential spectroscopic signatures of the planet's atmosphere, and in Sect. 6 we derive upper limits on the detection of starlight reflected by the planet. Finally, in Sect. 7 we summarise the results, discuss their implications and suggest directions to extend our study in the future.

2. Observations

Spectropolarimetric data of HD 189733 were collected with ESPaDOnS and CFHT, during 2 separate runs in 2006 June (10–13) and August (05–12). With ESPaDOnS, the complete optical spectrum (from 370 to 1000 nm) is collected in a single exposure at a spectral resolution of about 65 000; from sequence of 4 subexposures taken in different configurations of the polarimeter, one can obtain both the intensity and polarisation spectrum, in either circular (Stokes V) or linear (Stokes Q or U) polarisation state (Donati et al. 1997; Donati 2007). Circular polarisation spectra give access to the Stokes V Zeeman signatures and thus to the longitudinal field component averaged over the visible stellar hemisphere; they allow us to retrieve the parent large-scale magnetic field at the surface of the star (see Sect. 3). Linear (Stokes Q and U) polarisation can potentially inform us of the amount of stellar light reflected off the dusty planetary atmosphere; this signal (whose typical size is of order a few tens of ppm with respect to the stellar flux and depends on the planet albedo) is expected to be modulated by the planet orbital phase (see Sect. 6) and to reach its maximum size near the planet orbital quadrature. Eight Stokes V sequences at 3 main epochs, and 7 Stokes V sequences at 6 main epochs were collected during the first and second run respectively, the 4 remaining sequences corresponding to Stokes Q and U sequences. Signal to noise ratios (S/N) range from 600 to 1100 per 2.6 km s^{-1} velocity bin, with typical values between 900 and 1000. The complete journal of observations is given in Table 2.

Orbital and rotational phases (listed in Table 2) were computed respectively using the ephemerides (see Winn et al. 2007a; Croll et al. 2007):

$$T_0 = \text{HJD } 2\,453\,988.80336 + 2.2185733E_{\text{orb}} \quad (1)$$

Table 2. Journal of spectropolarimetric observations. The successive columns list the sequence number (Col. 1), the UT date (Col. 2), the UT Heliocentric Julian date (Col. 3), the orbital phase (using ephemeris of Eq. (1), Col. 4), the rotational phase (using ephemeris of Eq. (2), Col. 5), the measured polarisation state (Col. 6), the total exposure time (Col. 7), the peak signal to noise ratio in the spectrum (per 2.6 km s⁻¹ velocity bin, Col. 8), the longitudinal magnetic field B_ℓ whenever Stokes V is measured (with corresponding 1 σ error bars, Col. 9), the equivalent width S_{Ca} of the residual emission core in the Ca II H&K line (Col. 10, see Sect. 4) and the radial velocity v_{rad} (Col. 11).

Seq. (#)	Date (UT)	HJD (2 453 000+)	ϕ_{orb}	ϕ_{rot}	Stokes	Exp. time (s)	Peak S/N (per pixel)	B_ℓ (G)	S_{Ca} (km s ⁻¹)	v_{rad} (km s ⁻¹)
1	2006 Jun. 10	897.01115	0.625	0.221	Q	4 × 960	980		-0.56	-2.105
2	2006 Jun. 10	897.05805	0.647	0.225	U	4 × 960	1040		-0.82	-2.089
3	2006 Jun. 11	897.95814	0.052	0.301	V	4 × 900	1080	+7.2 ± 0.6	-0.11	-2.292
4	2006 Jun. 11	898.00269	0.072	0.305	V	4 × 900	1000	+7.7 ± 0.7	-0.53	-2.321
5	2006 Jun. 11	898.04669	0.092	0.309	V	4 × 900	930	+7.9 ± 0.8	-0.16	-2.338
6	2006 Jun. 12	898.98463	0.515	0.388	V	4 × 900	830	+2.4 ± 0.8	+0.20	-2.191
7	2006 Jun. 12	899.03159	0.536	0.392	Q	4 × 1000	1040		+0.27	-2.166
8	2006 Jun. 12	899.08036	0.558	0.396	U	4 × 900	1140		+0.11	-2.154
9	2006 Jun. 13	899.99747	0.971	0.474	V	4 × 730	890	-8.5 ± 0.8	+0.43	-2.198
10	2006 Jun. 13	900.04204	0.992	0.478	V	4 × 846	1000	-6.3 ± 0.7	+0.55	-2.204
11	2006 Jun. 13	900.08354	0.010	0.481	V	4 × 846	960	-8.3 ± 0.7	+0.73	-2.274
12	2006 Jun. 13	900.12387	0.028	0.485	V	4 × 600	790	-6.9 ± 0.9	+0.36	-2.279
13	2006 Aug. 05	952.86578	0.801	0.954	V	4×350	620	+2.1 ± 1.1	-0.57	-1.922
14	2006 Aug. 05	952.88433	0.810	0.956	V	4×275	560	+0.9 ± 1.3	-0.99	-1.928
15	2006 Aug. 08	955.90633	0.172	0.212	V	4×715	900	-4.1 ± 0.8	-0.20	-2.306
16	2006 Aug. 09	956.90905	0.624	0.297	V	4×1050	1120	+0.2 ± 0.6	-0.69	-1.996
17	2006 Aug. 10	957.90042	0.071	0.381	V	4×900	1050	+2.1 ± 0.7	+0.32	-2.214
18	2006 Aug. 11	958.91094	0.526	0.467	V	4×880	1030	+3.2 ± 0.7	+0.75	-2.112
19	2006 Aug. 12	959.91103	0.977	0.551	V	4×880	980	+2.8 ± 0.7	+0.78	-2.111

$$T_0 = \text{HJD } 2\,453\,988.80336 + 11.8E_{\text{rot}}. \quad (2)$$

A full planet transit was observed on June 13, with sequences 10 and 11 corresponding to transit (i.e. orbital phase equal to 0.0 ± 0.017), while sequences 9 and 12 correspond to phase ranges immediately preceding and following transit.

The raw data were reduced using Libre-ESPRIT, the dedicated and fully automatic spectropolarimetric reduction package available to ESPaDOnS users at CFHT (Donati et al. 1997; Donati 2007). From collected calibration exposures and stellar frames, Libre-ESPRIT automatically extracts wavelength-calibrated intensity and polarisation spectra with associated error bars at each wavelength pixel, shifted to the heliocentric rest frame and normalised to a unit continuum. In particular, all spectra are automatically corrected for spectral shifts resulting from instrumental effects (e.g. mechanical flexure, temperature or pressure variations) using the numerous telluric lines present in each spectra as a stable wavelength reference. Through cross-correlation, we estimate the relative shift of telluric lines with respect to the observer's frame; we assume that this shift is entirely attributable to instrumental effects and simply remove it by translating the spectra and recenter the telluric lines in the observer's rest frame. This is of course only an approximation; telluric lines are actually not a perfectly stable reference in the observer's rest frame, eg due to the effect of strong winds in the upper atmosphere (where telluric lines form) that can potentially shift these lines by as much as a few tens of m s⁻¹. In practice, we find that our method yields a radial velocity differential rms precision of about 15 m s⁻¹ within a single run, with systematic shifts of up to 30 m s⁻¹ from run to run (Donati 2007). This method is less accurate than the classical technique which consists in recording the spectrum of a reference ThAr lamp simultaneously (and interleaved) with that of the main star, yielding typical differential radial velocity accuracies of a few m s⁻¹; our method is nonetheless accurate enough to detect the planet-induced radial velocity variations of HD 189733 (see

below) and to ensure a reliable rotational modulation analysis of the detected Zeeman signatures (see Sect. 3).

Least-Squares Deconvolution (LSD, Donati et al. 1997) was applied to all spectra, using a line pattern derived from a Kurucz model atmosphere with solar abundances, and effective temperature and logarithmic gravity set to 5000 K and 4.5 respectively. This line pattern includes most moderate to strong lines present in the optical domain (those exhibiting central depths larger than 40% of the local continuum, before any macroturbulent or rotational broadening, about 7000 throughout the whole spectral range) but excludes the very strongest, broadest features such as the Balmer lines, whose Zeeman signature is strongly smeared out compared to those of narrow lines. The output of LSD for each sequence of polarisation spectra is a pair of average line profiles: either intensity (Stokes I) and circular (Stokes V) polarisation profiles, or linear (Stokes Q and U) polarisation profiles, depending on the type of observation sequence. We will refer to these as LSD profiles throughout the paper. The typical multiplex gain in S/N for polarisation profiles is 30, implying noise levels in LSD polarisation profiles as low as 30 to 40 ppm (i.e. 3 to 4×10^{-5} in units of the unpolarised continuum) depending essentially on the input spectrum quality. An example of such profiles is shown in Fig. 1.

Stokes V Zeeman signatures are detected for all circular polarisation observations (15 profiles altogether). From the first moment of the Stokes V LSD profiles, we derived estimates of the line-of-sight component of the magnetic vector averaged over the visible stellar hemisphere, ie the so-called longitudinal field B_ℓ (Donati et al. 1997). The values obtained are listed in Table 2 and typically range from -8 to $+8$ G. Note that longitudinal field values only represent a small fraction of the information stored in Stokes V profiles. For example, while the Stokes V signature corresponding to sequence 16 is clearly detected, featuring a signal with a full amplitude of 0.06% (i.e. 20 times larger than the corresponding error bar), the corresponding longitudinal field value is consistent with 0 G within the noise level and is thus unable to diagnose properly the field detection we obtained.

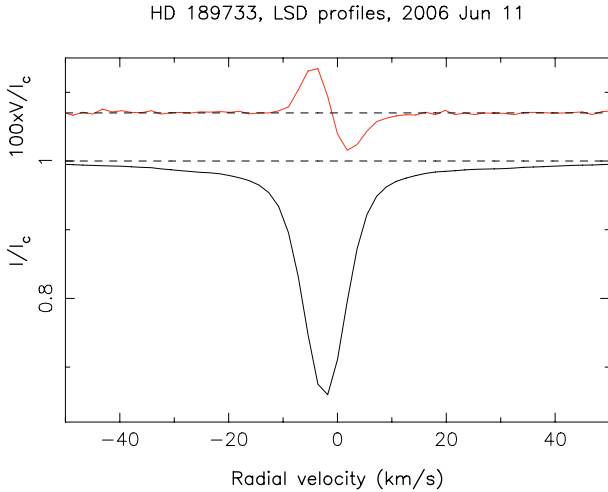


Fig. 1. LSD unpolarised (*bottom*) and circularly polarised (*top*) profiles of HD 189733 on 2006 June 11. All LSD profiles obtained on this night (corresponding to observation sequences 3 to 5, see Table 2) were averaged together, further decreasing the relative noise level (in the polarisation profile) down to 19 ppm. In this particular example, the full amplitude of the Stokes V signal is 0.12%, i.e. 60 times greater than the rms noise level. A Zeeman signature is obviously detected, corresponding to a longitudinal field value of about 8 G. Note that the Stokes V profile was expanded by 100 and shifted upwards for graphics purposes.

Nonetheless, longitudinal-field values are convenient summary statistics in several respects, and in particular can provide useful estimates of the average magnetic flux over the stellar surface when the field polarity is roughly uniform over the visible stellar hemisphere. In particular, these values indicate straightforwardly (and not unexpectedly) that B_ℓ correlates very poorly with orbital phase. Sequences 3 and 12, for example, correspond to very similar orbital configurations, but yield widely discrepant B_ℓ values. On the other hand, B_ℓ varies rather smoothly with stellar rotation phase, changing from positive to negative values throughout the first observing run. A more complete modeling of the magnetic topology from our collection of LSD Stokes V profiles is presented in Sect. 3.

From Gaussian fits to each LSD Stokes I profile, we derive radial velocities of HD 189733 throughout our 2 runs. The values we obtain (listed in Table 2) are in good agreement with expectations (using the orbital solution of Bouchy et al. 2005; and the ephemeris of Winn et al. 2007a, given in Eq. (1)) once the data are globally shifted by -0.13 km s^{-1} and -0.23 km s^{-1} for the June and August sets respectively (see plot in Fig. 2). Residuals to the model are equal to 15 and 10 m s^{-1} rms for the June and August run respectively, confirming that this is indeed the typical radial velocity differential accuracy that ESPaDOnS can reach. While the global shift of about 0.2 km s^{-1} between the ESPaDOnS and the ELODIE data (Bouchy et al. 2005) may be attributable to differences in the radial velocity calibration procedures between the 2 instruments, the 100 m s^{-1} relative shift between our June and August data sets is significantly larger than the upper limit corresponding to the long-term stability of ESPaDOnS (about 30 m s^{-1}). It suggests that HD 189733 could host more than one giant planet and feature at least another one at a typical distance of 0.5 AU. This will be investigated through future long-term spectroscopic monitoring.

Finally, we perform a bisector analysis from normalised LSD Stokes I profiles and measure the bisector span, from average velocities corresponding to 10–40% and 55–85% of the full LSD

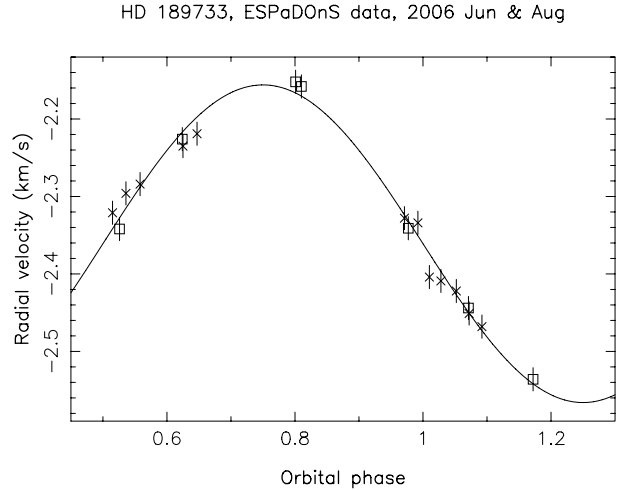


Fig. 2. Radial velocities of HD 189733 derived from ESPaDOnS spectra collected in 2006 June (crosses) and August (squares) as a function of orbital phase (using the ephemeris of Eq. (1)). The radial velocity model of Bouchy et al. (2005) is also plotted (full line). Note that the measurements were shifted by -0.13 km s^{-1} and -0.23 km s^{-1} for the June and August data respectively, to compensate for a global shift with respect to the model predictions (see text). Individual $1-\sigma$ error bars of 15 m s^{-1} are also plotted. Note that the deviating point near phase 1.0 is compatible with the Rossiter-McLaughlin effect (Bouchy et al. 2005; Winn et al. 2007a).

profile depth. The error bar on the bisector span is generally of the order of the error bar on the radial velocity estimate, about 15 m/s in the present case.

3. Modeling the magnetic topology of HD 189733

To model the magnetic topology of HD 189733, we use our magnetic-imaging code (Brown et al. 1991; Donati & Brown 1997) in its most recent implementation (Donati et al. 2006). While still based on maximum-entropy image reconstruction, this latest version reconstructs the field topology as a spherical-harmonic decomposition, rather than as a series of independent magnetic-image pixels. One obvious advantage of this method is that we can impose a priori constraints on the field topology – e.g., that the field is purely poloidal, or purely toroidal, or more generally, a combination of both. Another important advantage of this formalism is that both simple and complex magnetic topologies can easily be reconstructed (Donati et al. 2006), whereas the original method failed at reconstructing simple magnetic geometries (such as dipoles; Brown et al. 1991). Details about how we effected this approach are given in Donati et al. (2006). In this section, we assume that the Stokes V profiles are modulated with the rotation period of 11.8 d; we further assume that the rotation spin axis of the star coincides with the orbital axis, inclined at 85.7° with respect to the line of sight¹.

To describe the LSD Stokes V profiles of HD 189733, we use the same simple model of Donati et al. (1997) and

¹ While Winn et al. (2007a) find that the spin and orbit axis are most likely aligned in HD 189733, Croll et al. (2007) conclude in favour of a moderate spin-orbit misalignment from their very accurate photometric data set. However, the latter mention that their result only holds if no differential rotation is present at the surface of the star, an assumption whose validity is fairly uncertain (see end of Sect. 3). We thus assume here that the spin and orbit are aligned; a 20° change in the assumed inclination has however very limited impact on the derived magnetic topology.

Donati et al. (2006). In this model, the local unpolarised line profile is described with a Gaussian, whose full-width-at-half-maximum is set to 7 km s^{-1} and whose equivalent width matches that of the observed LSD Stokes I profiles (3.2 km s^{-1}); integrating over the stellar surface and taking $v \sin i = 3.0 \text{ km s}^{-1}$ (Winn et al. 2007a) enables us to reproduce the observed Stokes I profiles fairly well, once the model profiles are broadened with an instrumental broadening of 4.6 km s^{-1} . We then assume that the local Stokes V profile is proportional to the first derivative of the local Stokes I profile (weak field approximation), the scaling factor depending in particular on the local longitudinal field component and the Landé factor of the average line (set here to 1.25). For more details, the reader should refer to Donati et al. (1997).

Given the fairly low $v \sin i$ of HD 189733, it is obvious that the spatial resolution we can achieve at the surface of the star is rather limited. From the width of the local line profile (about 7 km s^{-1}), we derive that there are about 3 resolution elements across the stellar equator, implying that using spherical harmonics expansions with $\ell \leq 5$ is sufficient for our needs. It also implies that most small-scale magnetic features potentially present at the surface of HD 189733, e.g., in the form of small bipolar spot groups like those peppering the surface of the Sun, will remain totally undetected in spectropolarimetric data sets; this reflects the fact that close-by opposite magnetic polarities mutually cancel their respective effect in the Zeeman polarised signatures, that are sensitive to the vector properties of the field.

The maximum-entropy fits we obtain in this context for each of our 2 data sets are shown in Fig. 3, while the corresponding maps (assuming a magnetic field featuring both poloidal and toroidal components) are shown in Fig. 4. Both data sets are fitted down to the noise level and correspond to a reduced χ^2 of order unity. Note that in both cases, the data set is only fragmentary, covering no more than 20% and 50% of the rotation cycle for the June and August sets respectively. It explains in particular why only little magnetic flux is reconstructed at the stellar surface in regions not (or only marginally) constrained by observations. This is due to the fact that the imaging code is tailored to produce the simplest surface magnetic topology compatible with the data; it therefore spontaneously biases the solution towards topologies featuring little magnetic flux on poorly observed regions of the stellar surface, provided that (i) this is compatible with observations at other rotational phases and that (ii) the assumed field topology is complex enough to allow a mixture of non-magnetic and magnetic regions (i.e., the spherical harmonics expansion describing the field topology includes orders significantly larger than 1). For this reason, we emphasise that the modeling we carry out in this paper is only preliminary and deserves further confirmation and assessment through more complete data sets. However, a number of reliable conclusions can be derived already from the present data.

The first point we can address concerns the topology of the field. By trying to fit the data with different field configurations (e.g. a poloidal field only, or a general poloidal plus toroidal field combination), one can check which topology is more likely to be present at the surface of the star. In the present case, we find that the field of HD 189733 most probably features both a poloidal and a toroidal component at the surface of the star. Although both options give equivalent likelihoods in terms of the quality of fit to the data, the inclusion of a toroidal field component produces a magnetic configuration with significantly lower contrast (hence greater entropy and higher prior probability), yielding a higher posterior probability. This is particularly obvious for the August data set, for which the poloidal plus toroidal field

configuration that fits the data at the noise level is almost twice as weak on average as that obtained when assuming that the star hosts a purely poloidal field (not shown here). This conclusion can be inferred straightforwardly from the corresponding Stokes V data set (see Fig. 3). At this epoch, the mean Stokes V profile averaged over the whole series, as well as more than half of the individual profiles (e.g. that at phase 0.620), are clearly more-or-less symmetric about the line center. This is the characteristic signature of an azimuthal field ring encircling most of the star (e.g., Petit et al. 2005). The same conclusion may be deduced from the June data set, although the evidence is weaker than for the other (more complete) data set. In particular, the portions of the azimuthal field ring reconstructed at both epochs feature the same (ie clockwise or negative) polarity (see Fig. 4), strengthening the evidence that this toroidal field ring is indeed a real component of the magnetic topology of HD 189733.

We can also be fairly confident that the magnetic field at the surface of the star is significantly more complex than that of the Sun. Magnetic field models with a spherical harmonic expansions restricted to $\ell \leq 2$ produce significantly worse fits to the August data set, with reduced χ^2 values always larger than 2.5.

The modulation of the Zeeman signature on the August run looks very different from the regular shift from one main polarity to the other in about half a rotation period (as observed from most chemically peculiar stars, Wade et al. 2000a) that a simple dipolar-like topology would produce. Similarly, we observe in June a complete transition from one polarity to another in no more than 15% of the rotation cycle, which again cannot be reconciled with a simple dipolar-like magnetic topology. This is also straightforwardly visible from the longitudinal field values that we obtain (see Table 2), whose temporal variation is inconsistent with expectations from a simple field topology (e.g., Wade et al. 2000b). Although the data at both epochs are too sparse to give a definitive picture of the global magnetic topology, we can nevertheless infer that it includes several (presumably radial) magnetic field spots of opposite polarities across the equator. The typical magnetic intensity within these spots is a few tens of G (and possibly up to 40 G in the azimuthal field ring), significantly greater than the large-scale field strength of the Sun (about 5 G at the pole).

Further evidence of complexity comes from the apparent variability of the field topology on a time scale of a few weeks. This is directly visible on the reconstructed maps, where the magnetic spot distributions at both epochs share little in common. Although this is not totally unexpected given the very incomplete phase coverage, this is also the case around phase 0.50, a portion of the stellar surface that was covered at both epochs. This is particularly obvious in the Zeeman signatures collected around phase 0.48 in 2006 June, which are obviously incompatible (both in shape and polarity) with that obtained at phase 0.47 in 2006 August and with those obtained at nearby phases (0.38 and 0.55). This is further confirmed by trying to fit simultaneously both data sets with a single field topology. No acceptable fit to the data can be obtained for values of the period ranging from 11 to 14 d. Reduced χ^2 values lower than 2 can only be obtained for some rotation periods between 12.2 and 13.4 d. For a period of 12.2 d, for instance, the Zeeman signatures at phases 0.47 and 0.55 in the August data set are approximately matched with those at phases 0.30 and 0.38 in the July data set. We must therefore conclude that the magnetic topology evolved significantly between our two runs, e.g., under the effect of differential rotation. If we assume that the variability was not so large as to render the magnetic topologies at both epochs fully uncorrelated, we find (by minimising the misfit between the two data sets) that

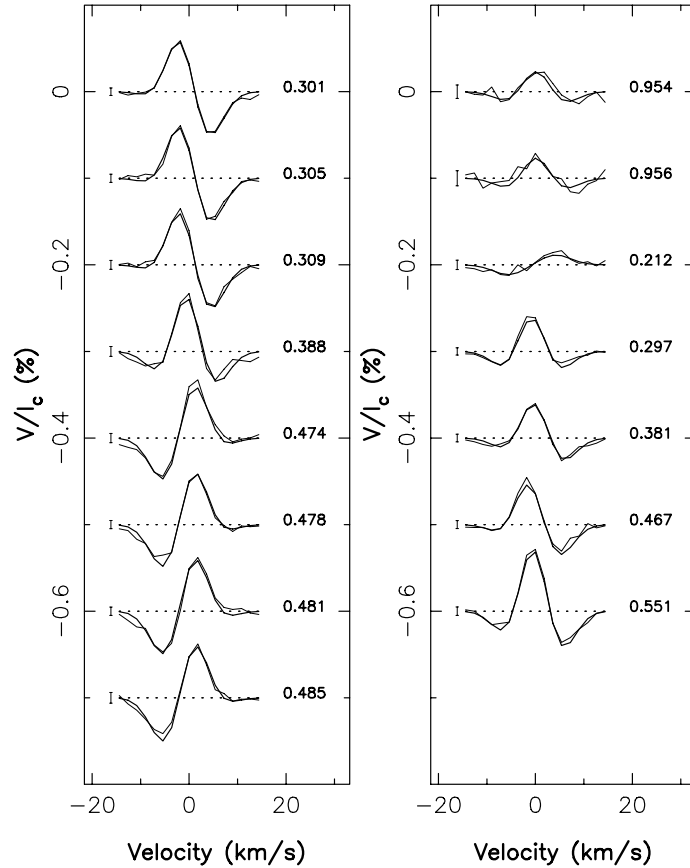


Fig. 3. LSD Stokes V profiles of HD 189733 (thin line) and corresponding maximum-entropy fit (thick line) for our 2006 June (*left panel*) and August (*right panel*) data sets. The rotational phases of observations (as derived from the ephemeris of Eq. (2)) are noted to the right of each profile. A $3\text{-}\sigma$ error bar is also depicted to the left of each profile.

the average recurrence period of the Zeeman signatures must be significantly longer than 11.8 d.

This latter conclusion confirms reports in the literature from photometric monitoring that variations in light-curve morphology occur on HD 189733 on timescales of a few tens of days. As far as our data indicate, the recurrence period of the Zeeman signatures is longer than the 11.73-day period retrieved by Croll et al. (2007), but shorter than the 13.4-d period found by Winn et al. (2007a). We suspect that all these discrepant periods actually reflect the fact that HD 189733 is differentially rotating; the recurrence period derived from the various data sets traces essentially the rotation period at the latitudes of the main brightness/magnetic features that are present at the surface of the star at the time of the observations. For instance, all data sets could potentially be reconciled by assuming that the equator and pole of HD 189733 are rotating with periods of 11.8 and 13.5 d respectively, i.e., a latitudinal photospheric shear similar to that of the Sun. Providing this is indeed the correct interpretation, it would imply that differential rotation at the surface of HD 189733 is at least as strong as that of the Sun, i.e., with a lap time between the equator and pole of less than 100 d. Additional observations are obviously needed to confirm this option; spectropolarimetric data collected over a timescale of about 15 d could settle this issue fairly easily.

4. Intrinsic stellar vs planet-induced activity

HD 189733 is known as a variable star. Its S_{HK} index value is 0.525 from the catalog of Wright et al. (2004), implying that

HD 189733 is among the 10% most active K dwarfs of the catalog, and among the 20% most active stars of the whole catalog (including 1200 stars altogether). To investigate how the activity of HD 189733 varies with time, we searched the emission cores in the Ca II H&K lines for potential variability. To maximise the accuracy, we computed a mean profile from both Ca II H&K lines at each phase, and subtracted from each profile the average over the whole data set. The resulting residuals are shown in Fig. 5. Variations of up to $\pm 10\%$ of the core emission flux are observed throughout both runs. Changes in the amount of core emission are derived by measuring the equivalent widths of the residual profiles of Fig. 5. The corresponding values are listed in Table 2 and plotted in Fig. 6. When the H and K lines are treated separately, the same behaviour is observed in both cores, with similar amplitudes.

The first obvious (and unsurprising) finding is that the activity of HD 189733 (as witnessed through the Ca II H&K emission cores) is intrinsically variable on time scales as short as 1 h. On June 11 for instance, the activity noticeably increased between the first and second polarisation sequences, then dropped again on the third polarisation sequence. This sudden burst of activity is probably due to a small flare triggered by a local reconnection event; it is however impossible at this stage to speculate about the cause of this event given the very sparse data sampling that we have.

The longer-term variations in core emission are apparently not related to the orbital phase, as one can also see fairly clearly from Table 2. While the activity is lower than average on June 11 (just after the transit), it is much stronger than average about

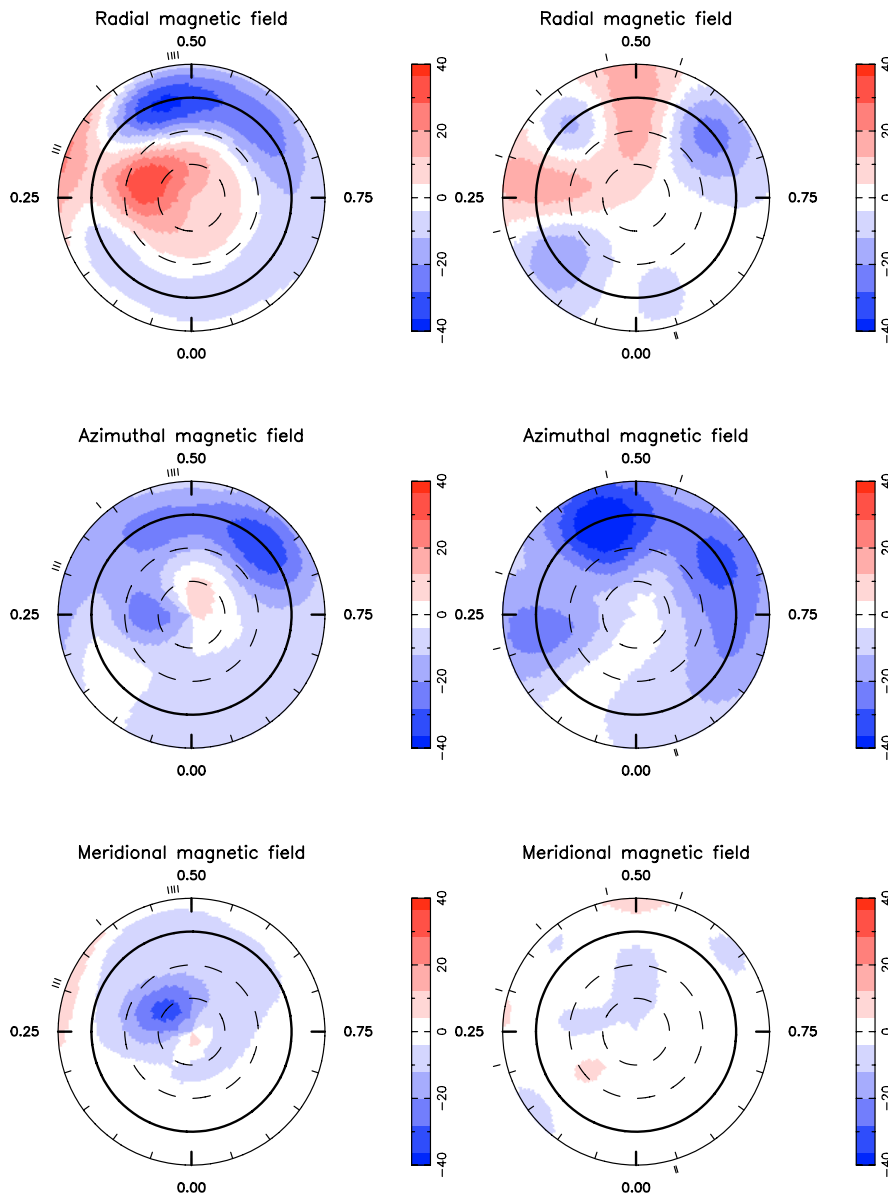


Fig. 4. Maximum-entropy reconstructions of the magnetic topology of HD 189733 as derived from our 2006 June (*left panel*) and August (*right panel*) data sets, assuming that the global field can be expressed as the sum of a poloidal field and a toroidal field. The three components of the field are displayed from top to bottom (flux values labelled in G). The star is shown in flattened polar projection down to latitudes of -30° , with the equator depicted as a bold circle and parallels as dashed circles. Radial ticks around each plot indicate phases of observations (as derived from the ephemeris of Eq. (2)).

2 days later, both before, during and after the transit. More generally, very little correlation is observed between the activity level and the orbital phase, for either data set. Activity correlates significantly better with stellar rotation phase (see Fig. 6), though intrinsic variability generates a significant dispersion of data points. Figure 7 shows a fit to the nightly-averaged June data (top panel), describing the average rotational modulation in the activity level of HD 189733. Residuals with respect to this average rotational modulation are plotted against the planet orbital phase in Fig. 7 (lower panels). These residuals both show a large dispersion of individual measurements and no obvious correlation with the planet orbital phase. The available phase sampling is however still insufficient; we thus cannot conclude from our data whether the planet is responsible for activity enhancement along the interaction models proposed in the literature (Cranmer & Saar 2007; McIvor et al. 2006).

The variations in Ca II H&K emission with stellar rotation phase appear to be in good mutual agreement for both runs (see Fig. 6). Since the activity presumably relates to the large-scale magnetic topology, it suggests that the intrinsic variability of the field structure as detected through the change in the Zeeman signatures (see Sect. 3) is only moderate and local, leaving the global field mostly unaffected. It also suggests that the rotation period at the footpoints of the magnetic loops that confine and heat the chromospheric plasma to produce the observed Ca II H&K emission is close to 11.8 d, i.e. consistent with that derived from the MOST photometric data (Croll et al. 2007) but smaller than the recurrence timescale derived from the Zeeman signatures themselves. This is not necessarily inconsistent; Zeeman signatures likely trace both open and closed magnetic field lines, while Ca II emission senses mostly closed field lines. Assuming that closed field lines concentrate

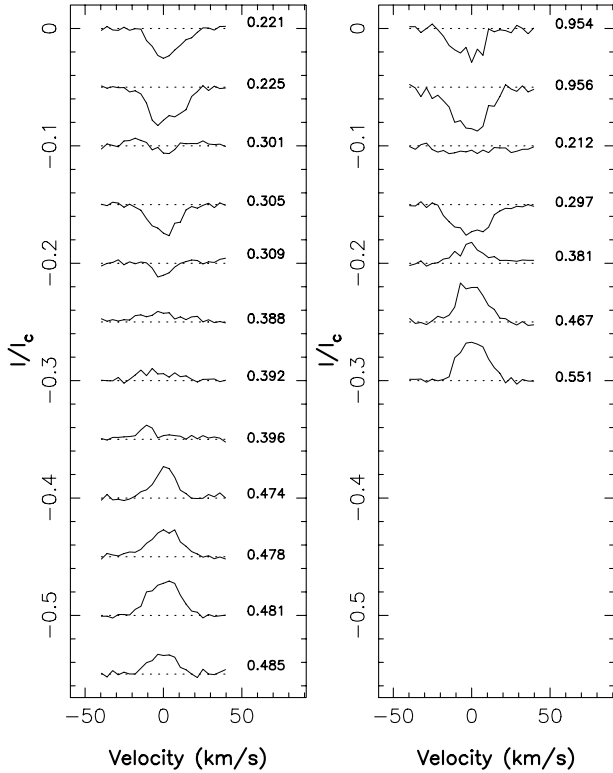


Fig. 5. Evolution of Ca II H&K residual intensity in the emission core (in units of the unpolarised continuum), for both the 2006 June (*left panel*) and August (*right panel*) data set. The corresponding rotation phase is indicated to the right of each profile.

around the equator in HD 189733 (as they do in the Sun), this would argue for a pole rotating slower than the equator in HD 189733.

Given the incompleteness of our data, these conclusions are of course very uncertain; they will however be testable as soon as a data set covering the whole stellar rotation cycle is obtained.

Folding the Ca II H&K emission variations on half the planet’s orbital period (i.e. 1.109 d) produces a correlation similar to that of Fig. 6. However, this apparent correlation is presumably the fictitious result of aliasing between the stellar rotation period and the length of the sidereal day. Given the sampling of our observations (i.e. roughly one series per day at fixed time, within about ± 2 h), modulation on a period of 11.8 d (producing a phase shift of $+8.5 \pm 0.7\%$ of the rotation cycle from one day to the next) generates a similar pattern to modulation on a period of 1.109 d (producing a phase shift of $-10 \pm 7\%$ for two successive observations). The phase diagram by itself is thus not sufficient to determine on which timescale activity is modulated. However, if activity was truly modulated on a 1.109 d period, e.g. due to tidal effects induced by the planet, we would then expect other activity indices (e.g. photometry tracing surface starspots) to show a similar behaviour; according to Winn et al. (2007a) and Croll et al. (2007), no modulation on a 1.109 d timescale is observed in their densely-sampled photometric data. We thus conclude that most of the activity of HD 189733 traced by the Ca II emission core is likely varying with the stellar rotation period.

Note that we do not suggest that activity is completely independent of orbital phase in HD 189733; while the largest fraction of the activity level is likely driven by conventional activity processes (and thus modulated by the star’s rotation), it may

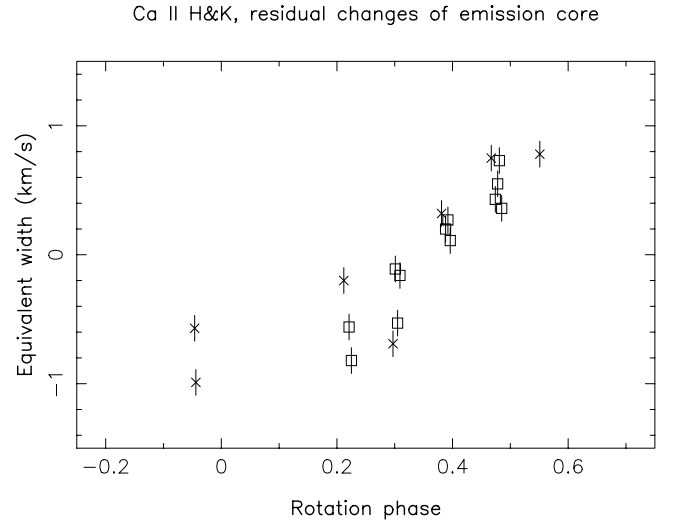


Fig. 6. Equivalent width variations in the emission cores of the Ca II H&K lines as a function of rotation phase (derived from the ephemeris of Eq. (2)), for both the 2006 June (crosses) and August (open squares) data sets. The equivalent width of the average emission core is equal to 13 km s^{-1} in HD 189733.

well be that a small fraction of the observed activity is induced by the planet/star interaction. Given the high level of intrinsic variability characterising Ca II emission (see Fig. 6), this option can only be checked from observations featuring dense temporal sampling over both orbital and rotational periods.

5. Transmission spectrum

We now consider the transmission signature of the planet’s atmosphere in the intensity spectrum, i.e., the residual on-transit spectrum after the off-transit spectrum has been subtracted. One may expect absorption signatures from the planet atmosphere to be present in the transmission spectrum. Similar attempts to detect atmospheric spectral features from the ground have yielded null results on the system HD 209458 (Bundy & Marcy 2000; Moutou et al. 2001; Brown et al. 2002; Moutou et al. 2003; Snellen 2004; Deming et al. 2005), whereas space-based observations gave positive detections, at a level of 10^{-4} in the visible NaI doublet (Charbonneau et al. 2002) and probably stronger in the UV (Vidal-Madjar et al. 2003; Ballester et al. 2007).

The on-transit spectrum is the combination of all polarised spectra from sequences 10 and 11, i.e., in total 8 spectra of individual SNR more than 400 at 730 nm. The final combined on-transit spectrum is of SNR 550 to 1100, depending on the wavelength. In the off-transit comparison spectrum, we included all spectra of the transit night except sequences 10 and 11. Each spectrum has to be interpolated to a common spectral format before combination. The impact of this interpolation should be negligible on features broader than the spectral sampling interval. The resulting transmission spectrum does not show absorption features, at a level of 0.0012 relative flux in the region of the NaI doublet, and more generally, at a level between 0.001 and 0.003 over the available spectral range, from 369 nm to 1045 nm. Narrow NaI absorption features of 0.45% amplitude and 0.01 nm width, such as predicted by models of HD 209458 (Tinetti et al., in prep) are undetected.

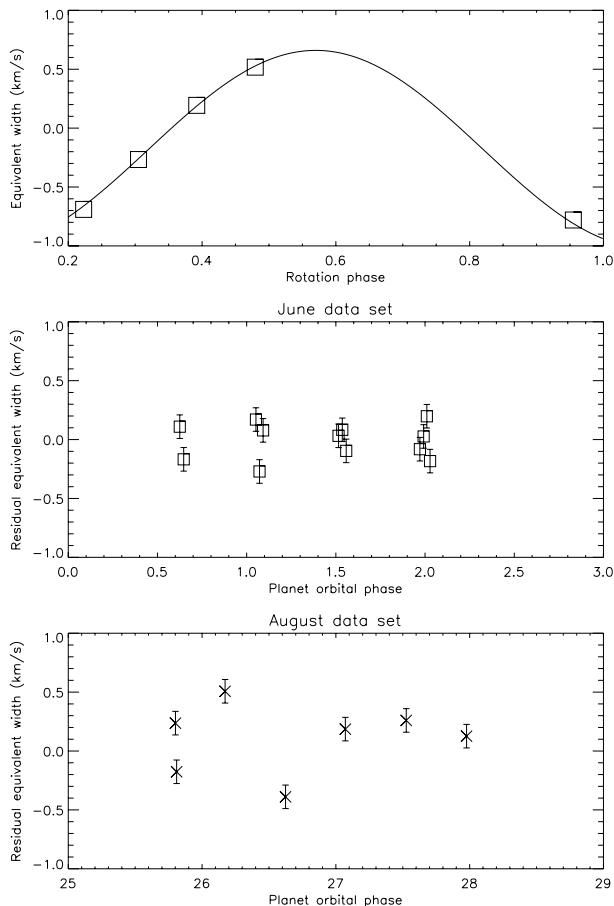


Fig. 7. Nightly averaged equivalent widths of the Ca II H&K lines of the June data set as a function of rotation phase fitted by a cosine rotational function (*top panel*); residuals of the individual Ca II equivalent widths after this correction is applied, as a function of the planet orbital phase (*middle panel* for the June data set and *top panel* for the August data set): the high dispersion shows the activity jitter, but at such temporal sampling no specific correlation with the planet motion is observed.

6. Planetary reflected-light spectrum

Finally, we searched our linear polarisation spectra for signatures of light from the star reflected off the planet’s atmosphere towards the observer. With a short semi-major axis (0.031 AU), a known planetary radius and the geometry of the system well constrained by transit observations, the system HD 189733 probably offers one of the most favorable configurations to constrain the albedo of a giant exoplanet. Upper limits on the albedos of hot Jupiters have been derived from similar searches on HD 75289, ν And and τ Boo, involving several tens of observing nights on 4 m to 8 m class telescopes (Charbonneau et al. 1999; Collier Cameron et al. 2002; Leigh et al. 2003b,a,c). Their conclusion is that the (assumed grey) albedos of hot Jupiters are apparently smaller than 0.12, i.e., much smaller than those of solar-system planets like Jupiter and Venus. In our case, the star-planet distance is the smallest among all hot Jupiters discovered to date orbiting stars bright enough for such observations. It thus maximises the strength of the expected reflected signal, making it larger, by at least a factor of about 2, than all systems previously observed. The star is however fainter, compensating at least partly for this advantage.

All previous attempts to detect this spectroscopic signal have been made using unpolarised light only. However, this signal

is expected to be linearly polarised (Seager et al. 2000; Stam et al. 2004) and can thus also be detected through Stokes Q and U spectra. Detecting this signal through broad-band polarimetry was recently attempted with the new PLANETPOL polarimeter (Hough et al. 2006), with which a potential signal from τ Boo was reported (Lucas et al. 2006) (at a level of about 10 ppm). Similar measurements can be performed through spectropolarimetry. Since the reflected spectrum is expected to be polarised and Doppler shifted as a result of the planet orbital motion, we expect to see tiny polarisation structures in the spectrum of HD 189733, oscillating about the main spectral lines of the host star and varying in strength with orbital phase. These polarisation signatures are expected to be maximum at quadrature, i.e., for scattering angles of about 90° .

Although spectropolarimetric signatures of exoplanets are potentially easier to identify unambiguously (thanks to their modulated Doppler shifts) than broadband polarisation, they are more difficult to detect because their amplitudes are significantly smaller, being reduced by approximately the relative depth of the average line profile. Given the planet’s size and orbital distance in the particular case of HD 189733b, we expect the relative broadband polarimetric signal to peak at about 50 ppm at most (assuming a grey albedo of 0.4); we thus expect the spectropolarimetric signal to reach about 15 ppm (the relative depth of the LSD profiles being 0.3) at orbital phases 0.75 and 0.25. For a grey albedo of 0.12, this signature is further reduced to a maximum size of only 5 ppm. Our Stokes Q and U spectra each show a relative noise level of 25 ppm; we thus need to accumulate between 60 and 600 of them to reach noise levels of 3 to 1 ppm, as is needed to detect the spectropolarimetric signal with a precision of at least 5σ for albedos ranging from 0.4 down to 0.12 respectively. No useful upper limit on the albedo can therefore be obtained from our single pair of linear polarisation spectra; a few tens of such observations (at the very least) are required to be able to derive a useful constraint.

7. Conclusion

HD 189733 is among the most studied planetary systems, with a short-period (2.2d) Jupiter-like planet transiting the disc of its bright parent star. At only 0.031 AU distance from its relatively active host star (a K dwarf featuring moderate rotation), the gaseous planet is embedded in the outer corona and the magnetosphere of the star.

In order to understand the complex relationships between a star and a closeby Jupiter-mass planet and in particular to investigate the possible interaction that could lead to planet-induced activity enhancements such as those recently reported in the literature, we decided to explore the extent and topology of the stellar magnetosphere of HD 189733. We used the ESPaDOoS spectropolarimeter at CFHT to look for circular polarisation Zeeman signatures in the line profiles of HD 189733 in 2006 June and August.

Zeeman signatures are clearly detected in all spectra, demonstrating that a magnetic field is indeed present at the surface of the star. The Zeeman signatures are not modulated with the planet’s orbital period; their temporal variation agrees better with the star’s rotational modulation, even though the full rotation cycle of about 11.8 d was not fully covered by our observations.

Assuming that the observed variation is mainly caused by rotational modulation, the detected Zeeman signatures indicate that a large-scale magnetic field of a few tens of G is present

at the surface of this relatively active K dwarf star. The reconstructed large-scale field topology is significantly more complex than the large scale field of the Sun, involving in particular a toroidal component and significant contributions from magnetic multipoles of order of at least 3. The magnetic topology is apparently evolving on timescales of a few rotation cycles; moreover, the recurrence timescale of the Zeeman signature over the full timescale of our observations is apparently longer than the estimated rotation period of 11.8 d. Both points suggest that significant differential rotation is present at the surface of the star.

The Ca II H & K lines clearly feature core emission, whose intensity varies by about 10% on a day-to-day basis. This variability is mostly modulated with the rotation cycle of 11.8 d and presents rapid episodes of intrinsic fluctuations. The overall modulation itself is roughly stable over the timescale of our observations.

At this stage, there is very little we can state concerning putative activity enhancements induced by the presence of the giant close-in exoplanet orbiting HD 189733. In particular, its potential contribution to Ca II H & K emission needs to be investigated through further data, densely sampling both rotation and orbital cycles, to determine unambiguously whether, and to which level, the activity of HD 189733 also fluctuates with the planet orbital period. Ultimately, studies such as ours should allow us to diagnose whether star-planet interactions rather result from star-planet magnetospheric friction (crucially involving the large-scale field of the host star) or from tidal effects (producing mainly comoving small-scale magnetic features with no need for a large-scale magnetic field on the host star); looking for correlations between the planet-induced excess activity and the presence (and topology) of the large-scale field should for instance inform us on which of these 2 processes are more likely to occur.

Acknowledgements. We thank the anonymous referee for constructive comments about an earlier version of this manuscript.

References

- Bakos, G. Á., Knutson, H., Pont, F., et al. 2006, *ApJ*, 650, 1160
 Ballester, G. E., Sing, D. K., & Herbert, F. 2007, *Nature*, 445, 511
 Bouchy, F., Udry, S., Mayor, M., et al. 2005, *A&A*, 444, L15
 Brown, S., Donati, J. F., Rees, D., & Semel, M. 1991, *A&A*, 250, 463
 Brown, T. M., Libbrecht, K. G., & Charbonneau, D. 2002, *PASP*, 114, 826
 Bundy, K., Marcy G. 2000, *PASP*, 112, 1421
 Catala, C., Donati, J. F., Shkolnik, E., Bohlender, D., & Alecian, E. 2007, *MNRAS*, 374, L42
 Charbonneau, D., Noyes, R. W., Korzennik, S. G., et al. 1999, *ApJ*, 522, L145
 Charbonneau, D., Brown, T. M., Noyes, R. W., & Gilliland, R. L. 2002, *ApJ*, 568, 377
 Collier Cameron, A., Horne, K., Penny, A., & Leigh, C. 2002, *MNRAS*, 330, 187
 Cranmer, S., Saar, S. 2007, *ArXiv Astrophysics e-prints*
 Croll, B., Matthews, J., & Walker, G. 2007, *ApJ*, submitted
 Cuntz, M., Saar, S. H., & Musielak, Z. E. 2000, *ApJ*, 533, L151
 Deming, D., Brown, T., Charbonneau, D., Harrington, J., & Richardson, L. 2005, *ApJ*, 622, 1149
 Donati, J. F. 2007, *MNRAS*, in prep
 Donati, J. F., & Brown S. 1997, *A&A*, 326, 1135
 Donati, J. F., Semel, M., Carter, B. D., Rees, D. E., & Collier Cameron, A., 1997, *MNRAS*, 291, 658
 Donati, J. F., Howarth, I., Jardine, M., et al. 2006, *MNRAS*, 370, 629
 Hall, D., 1991, in (eds.) I. Tuominen, D. Moss, & G. Rüdiger *The Sun and Cool Stars. Activity, Magnetism, Dynamos*, Lecture Notes in Physics 380 (Berlin: Springer Verlag), IAU Colloq., 130, 353
 Hébrard, G., & Lecavelier des Etangs, A. 2006, *A&A*, 445, 341
 Hough, J., Lucas, P., Bailey, J., et al. 2006, *PASP*, 118, 1305
 Ip, W. H., Kopp, A., & Hu, J. H. 2004, *ApJ*, 602, L53
 Kurucz, R. L. 2007, *ArXiv e-prints*, 704
 Leigh, C., Cameron, A. C., & Guillot, T. 2003a, *MNRAS*, 346, 890
 Leigh, C., Cameron, A. C., Horne, K., Penny, A., & James, D. 2003b, *MNRAS*, 344, 1271
 Leigh, C., Collier Cameron, A., Udry, S., et al., 2003c, *MNRAS*, 346, L16
 Lucas, P., Hough, J., & Bailey, J. 2006, in *Tenth Anniversary of 51 Peg-b: Status of and prospects for hot Jupiter studies*, ed. L. Arnold, F. Bouchy, C. Moutou, 334
 Matthews, J. 2007, *ApJ*, submitted
 McIvor, T., Jardine, M., & Holzwarth, V. 2006, *MNRAS*, 367, L1
 Moutou, C., Coustenis, A., Schneider, J., et al. 2001, *A&A*, 371, 260
 Moutou, C., Coustenis, A., Schneider, J., Queloz, D., & Mayor, M. 2003, *A&A*, 405, 341
 Petit, P., Donati, J. F., Aurière, M., et al. 2005, *MNRAS*, 361, 837
 Seager, S., Whitney, B., & Sasselov, D. 2000, *ApJ*, 540, 504
 Shkolnik, E., Walker, G. A. H., & Bohlender, D. A. 2003, *ApJ*, 597, 1092
 Shkolnik, E., Walker, G. A. H., Bohlender, D. A., Gu, P. G., & Kürster, M. 2005, *ApJ*, 622, 1075
 Snellen, I. 2004, *MNRAS*, 353, L1
 Stam, D., Hovenier, J., & Waters, L. 2004, *A&A*, 423, 663
 Vidal-Madjar, A., Lecavelier des Etangs, A., Désert, J. M., et al. 2003, *Nature*, 422, 143
 Wade, G., Donati, J. F., Landstreet, J., et al. 2000a, *MNRAS*, 313, 823
 Wade, G., Donati, J. F., Landstreet, J., et al. 2000b, *MNRAS*, 313, 851
 Walker, G. A. H., Matthews, J. M., Kuschnig, R., et al. 2006, in: L. Arnold, F. Bouchy, & C. Moutou, *Tenth Anniversary of 51 Peg-b: Status of and prospects for hot Jupiter studies*, (eds.) 267
 Winn, J. N., Holman, M. J., Henry, G. W., et al., 2007a, *ArXiv Astrophysics e-prints*
 Winn, J. N., Johnson, J. A., Marcy, G. W., et al., 2007b, *ApJ*, 653, L69
 Wright, J. T., Marcy, G. W., Butler, R. P., Vogt, S. S. 2004, *ApJS*, 152, 261